Two-dimensional Fourier-transform spectroscopy of potassium vapor

X. Dai, A. D. Bristow, D. Karaiskaj, and S. T. Cundiff*
JILA, University of Colorado and National Institute of Standards and Technology, Boulder, Colorado 80309-0440, USA
(Received 12 January 2010; published 3 November 2010)

Optical two-dimensional Fourier-transform (2DFT) spectroscopy is used to study the coherent optical response of potassium vapor in a thin transmission cell. Rephasing and nonrephasing spectra of the D_1 and D_2 transitions are obtained and compared to numerical simulations. Non-perturbative calculations using the optical Bloch equations give very good agreement with the experimental peak strengths and line shapes. Nonradiative Raman-like coherences are isolated using a different 2DFT projection. Comparison between the optical and Raman linewidths shows that dephasing is due to partially correlated energy fluctuations. Density-dependent measurements show distortion of 2DFT spectra due to pulse propagation effects.

DOI: 10.1103/PhysRevA.82.052503 PACS number(s): 32.30.Jc, 32.70.Jz

I. INTRODUCTION

Vapors of alkali-metal atoms have a relatively simple energy level diagram due to the single outer electron. Consequently, they are ideal systems for the study of light-matter interactions. Examples of this include recent ultracold [1] and electromagnetically induced transparency [2] experiments.

The dynamics of alkali metals have been captured by ultrafast transient optical measurements, revealing signals that have been attributed to the tri-level [3] and two-photon [3] photon echoes, propagation effects [4,5], quantum interference [4,6,7], and non-Markovian response [8,9].

Coherent continuous-wave and transient measurements often suffer from ambiguous interpretation, even in simple systems such as alkali-metal vapors. In these vapors the optical response is affected by interatomic interactions, pulse propagation, and contributions from nonradiative coherences, which have not been cleanly resolved.

Optical two-dimensional Fourier-transform (2DFT) spectroscopy has been shown to separate various quantum excitation pathways by spreading the spectrum of a coherent signal on a two-dimensional frequency plane [10]. A sophisticated time-domain technique, 2DFT spectroscopy measures the phase of a nonlinear signal, which is generated by the mixing of three excitation pulses by the third-order nonlinear response of the sample. By measuring the phase as one of the delays between the excitation pulse is precisely stepped, it is possible to determine the frequency (or frequencies) of any coherences that exist during the interval between the excitation pulses. The two frequency dimensions typically correspond to the spectrum of the emission and the Fourier transform with respect to the delay that is stepped. This description ignores many important nuances of the technique, but is given to provide a simplified introduction to the method.

Optical 2DFT spectroscopy has its origins in multidimensional nuclear magnetic resonance spectroscopy [11] using radio-frequency pulses, and has also been used to explore molecular vibrations with infrared laser pulses [12–15]. At optical frequencies, the principles of 2DFT spectroscopy have been demonstrated on rubidium vapor [16–18], although this technique has been more commonly applied to the study of coherent dynamics in molecules [19] and semiconductor nanostructures [20].

Several different 2DFT spectra can be produced, depending on the time ordering of the pulses and which time delay is scanned. The most common 2DFT spectra provide information about the dephasing of optical coherences, even in the presence of inhomogeneous broadening. Other 2DFT spectra can clearly isolate nonradiative "Raman"-type coherences between two levels that do not have a dipole moment between them, but have radiative transitions to another common state [21]. In 2DFT spectroscopy, these nonradiative coherences are created because the laser has sufficient bandwidth to excite both radiative transitions from the common state. In contrast, coherent anti-Stokes Raman spectroscopy (CARS), which is typically used to access Raman coherences, usually uses two lasers producing nanosecond pulses of different frequencies.

In this paper, we present a detailed study of the coherent optical response for the two coupled D lines of potassium vapor in a thin transmission cell. We use an actively stabilized apparatus to generate the phase locked beams. This apparatus is versatile so that, in addition to acquiring the common "rephasing" and "nonrephasing" 2DFT spectra, we can easily scan any of the beams to acquire other 2DFT spectra, such as one that isolates Raman coherences [21]. By comparing the width of the Raman peaks in this spectrum to those for the optical coherences in the rephasing spectrum, it is possible to determine the degree of correlation for the fluctuations of the energy levels that cause dephasing. Experimental results are compared to numerical simulations based on the optical Bloch equations, to provide complete interpretation of the observed optical features. Our simulations include finite pulse width effects and are not perturbative, thus they can capture effects due to higher-order susceptibilities. At higher atomic densities, we observe distortions of the spectra, which do not appear in the simulations, and which we ascribe to pulse propagation effects.

The prior work on atomic vapors (rubidium) used different experimental methods than those presented here. The first work used a pulse shaper to produce collinear beams and used phase cycling to separate out the 2DFT spectra [16]. More

*cundiffs@jila.colorado.edu

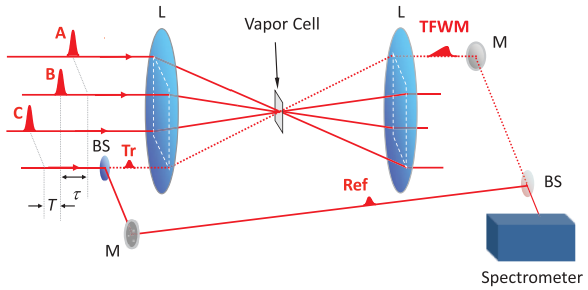

FIG. 1. (Color online) Schematic diagram of the experimental setup. Notation: L: lens, BS: beam splitter, M: mirror.

recent studies used a collinear geometry and acoustic-optic modulators to modulate the phase [18] or a diffractive pulse shaper to produce noncollinear pulses in a geometry similar to what we use, although the reference pulse went through the sample, rather than around it [17]. Only the second of these papers [18] provided a comparison to a perturbation theory that ignores finite pulse width effects, and none of them showed isolation of the nonradiative coherences.

II. EXPERIMENTAL

Optical 2DFT spectroscopy explicitly measures the phase of a transient four-wave mixing (TFWM) signal during two time periods of a three-pulse excitation sequence [22]. The resulting data is Fourier transformed onto a two-dimensional frequency plane, thus separating the electronic interactions between photoexcited states.

A mode-locked Ti:sapphire laser supplies ~200 fs pulses, centered at 768.2 nm to an ultrastable platform of nested and phase-controlled interferometers to generate four identical pulses arranged in a box geometry, i.e., the pulses propagate parallel to each other arranged on the four corners of a square in the plane perpendicular to the propagation direction [22]. A schematic of the four pulses and their use is shown in Fig. 1: three pulses (A, B, and C) are focused on the same spot of a home-made alkali-metal vapor cell and generate a TFWM signal from excitation of both the $4^2S_{1/2} \leftrightarrow 4^2P_{1/2}(D_1)$ and $4^2S_{1/2} \leftrightarrow 4^2P_{3/2}(D_2)$ transitions.

Time delays between the pulses are denoted τ, T, and t between the first and second, the second and third, and the third pulse and signal, respectively. Pulse four provides the phase-stabilized tracer (Tr) and reference (Ref) separately: the tracer copropagates with the TFWM signal and is useful for alignment, but is blocked during the 2DFT measurements; the reference beam is routed around the vapor cell and recombined with the signal, producing an interferogram that is recorded by a spectrometer that uses a cooled charged coupled device camera for detection. The phase of the signal field is determined by an all-optical method, which is realized by careful measurement of relative phases between all laser pulses and the TFWM signal [23]. Further experimental details can be found elsewhere [22,24].

The TFWM signal, $E_s \sim E_A^* E_B E_C$, is generated in the phase-matched direction $\mathbf{k}_s = -\mathbf{k}_A + \mathbf{k}_B + \mathbf{k}_C$ where E_A^* is the conjugated pulse. The subscripts, A, B, and C only denote direction, not time ordering. If E_A arrives first the resulting 2DFT spectrum, $S_I(\tau,T,t)$, is known as "rephasing" because the dephasing due to inhomogeneous broadening is canceled. In a TFWM experiment, this time ordering produces a photon echo. If E_A arrives second, the cancellation of dephasing due to inhomogeneous broadening does not occur, and the resulting $S_{II}(\tau,T,t)$ spectra are referred to as "nonrephasing." $S_{III}(\tau,T,t)$ spectra, where E_A arrives last, are sensitive to two-quantum resonances [25–27]. The time-resolved spectra $S_i(\tau,T,t)$ are usually Fourier transformed with respect to two time delays, while the third delay is fixed. The time delays τ and T are defined based on time ordering, not direction, and thus are strictly positive.

Reflection cells designed for high-temperature vapor experiments [28] cannot be used in our multidimensional spectroscopy apparatus, because the signal is detected in transmission [22]. Furthermore, in a reflection geometry the phase of the signal depends on the position of the interface producing the reflection. Therefore, a thin transmission cell for alkali atomic vapor has been designed and manufactured for the current experiment. The cell body is machined from high-grade titanium. Two sapphire windows are separately diffusion bonded to the titanium body. The gap between two windows, $L \sim 19\ \mu$m, can be adjusted before the transmission cell is loaded with solid potassium [28]. The vapor temperature is controlled by a heater attached to the transmission cell, up to a maximum of 800 °C. However, for the measurement reported here, the cell temperature is varied from 210 to 270 °C, ensuring low absorption and number densities in the range 2.03×10^{20} to 1.87×10^{21} m^{-3} [29]. During the measurements, the absorption spectrum of the potassium vapor at each temperature is recorded to estimate the gap size between two windows by comparing experimental spectra with calculated absorption spectra.

The measured linear absorption and the energy level diagram for atomic potassium are shown in Figs. 2(a) and 2(b), respectively. The laser excites both D_1 and D_2 transitions, and there are no resonant two-photon transitions. Figure 2(a) also shows the calculated linear absorption spectrum at 250 °C. At this temperature, the resonance broadened linewidths of the D_1 and D_2 transitions are below the spectrometer resolution. An argon buffer gas at ~1500 Torr pressure is added to the cell to induce collisional broadening. The argon reduces the absorbance αL below 1 into the weak absorption regime. In the calculation, the spectral linewidth is the sum of resonance from potassium-potassium interactions [30] and collisional broadening with argon [31].

III. RESULTS AND DISCUSSION

Figures 2(c) and 2(d) show the amplitude and real part of $S_I(\omega_\tau,T,\omega_t)$ and $S_{II}(\omega_\tau,T,\omega_t)$ 2DFT spectra of potassium vapor at 250 °C. The emission frequency ω_t is defined to be positive, thus for $S_I(\omega_\tau,T,\omega_t)$, the signal appears at negative ω_τ because the first pulse is conjugated. The $S_I(\omega_\tau,T,\omega_t)$ and $S_{II}(\omega_\tau,T,\omega_t)$ spectra can be used to determine homogeneous and inhomogeneous linewidths [32–34]. The horizontal axis of the spectrum is generated directly from the recorded interferogram between the reference pulse and the TFWM signal [35] at each delay step between the pulses A and B. The vertical axis of the spectrum is generated by fast Fourier transform with respect to τ. During the measurements, T was

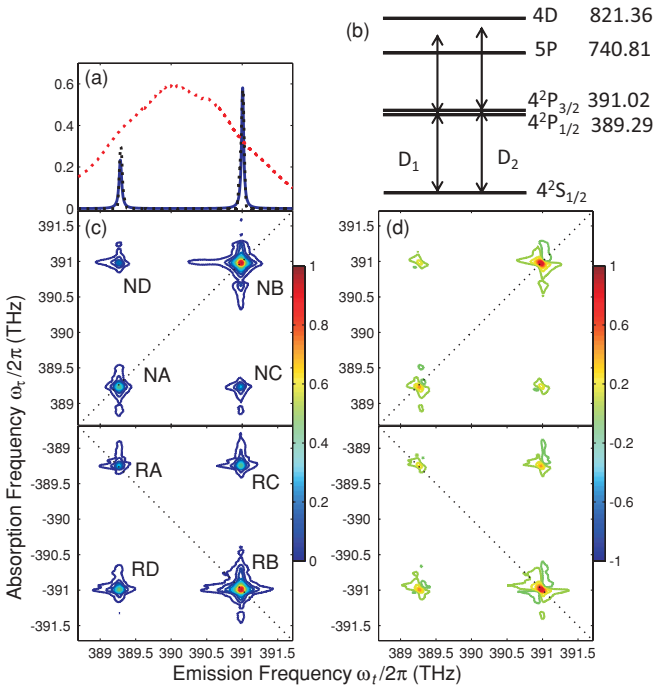

FIG. 2. (Color) (a) Excitation pulse spectrum (red dashed) and experimental (black dotted) and calculated (blue solid) linear absorption of potassium vapor at 250 °C. α is the absorption coefficient and L is the gap between the two sapphire windows. (b) Relevant energy levels of atomic potassium, with frequencies in THz. (c) Experimental amplitude rephasing spectrum $S_I(\omega_\tau,T,\omega_t)$ (bottom) and nonrephasing spectrum $S_{II}(\omega_\tau,T,\omega_t)$ (top) of potassium vapor. (d) Experimental real-part $S_I(\omega_\tau,T,\omega_t)$ (bottom) and $S_{II}(\omega_\tau,T,\omega_t)$ (top) spectra. The spectra are normalized to the most intense peak.

set to 580 fs, which is equal to $1/(f_{D2}-f_{D1})$ where f_{D1} and f_{D2} are the transitions frequencies corresponding to the transitions D_1 and D_2, respectively.

Each spectrum has two diagonal peaks, which correspond to the D_1 and D_2 transitions, and two off-diagonal peaks, which represent coupling between the two resonances. However, the relative peak strengths are different in $S_I(\omega_\tau,T,\omega_t)$ and $S_{II}(\omega_\tau,T,\omega_t)$ spectra. This difference can be qualitatively explained by the double-sided Feynman diagrams shown in Fig. 3. Double-sided Feynman diagrams are useful for illustrating all possible Liouville-space pathways in the systems [10]. Two pathways contribute to each peak in the $S_I(\omega_\tau,T,\omega_t)$ spectra; whereas for $S_{II}(\omega_\tau,T,\omega_t)$ three pathways contribute to each diagonal peak (NA or NB) and only one pathway to each cross peak (NC or ND). Generally, the peak strengths are proportional to the sum over participating diagrams, while the strength of an individual diagram is proportional to $\Pi\mu_i$, where index i runs from 1 to 4 and μ_i is the transition dipole moment for each excitation step in each double-sided Feynman diagram. The ratio between the transition dipole moment for the D_2 transition, μ_{D2}, to the dipole moment for D_1 transition, μ_{D1}, is approximately $\sqrt{2}:1$. Assuming each quantum pathway has the same contribution to the peak strength, the peak strength ratio RA:RC:RD:RB is proportional to $2\mu_{D1}^4 : 2\mu_{D1}^2\mu_{D2}^2 : 2\mu_{D2}^2\mu_{D1}^2 : 2\mu_{D2}^4$, or

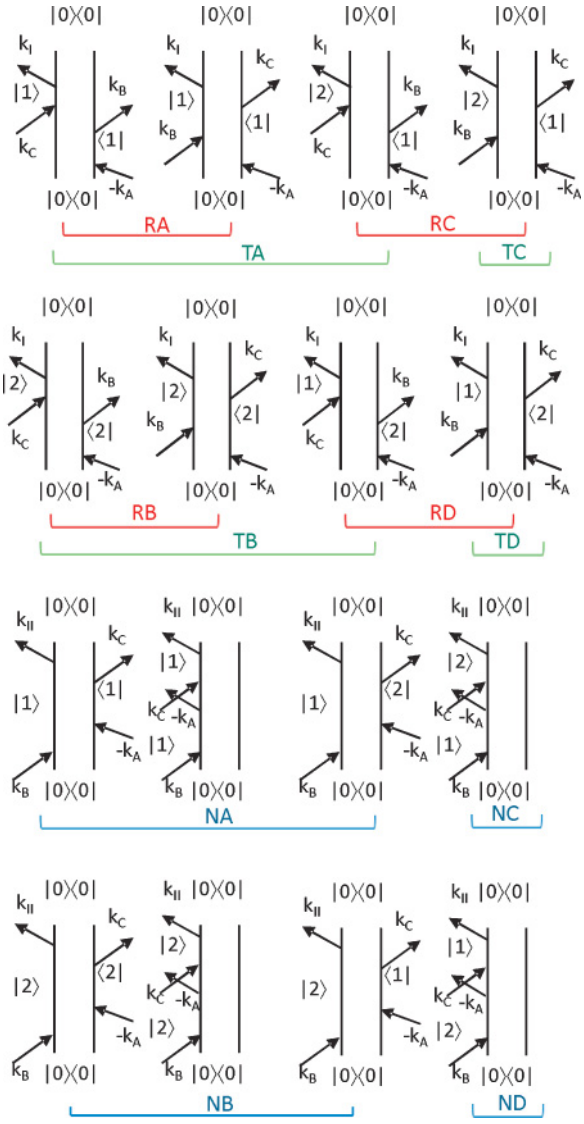

FIG. 3. (Color online) Double-sided Feynman diagrams for all possible Liouville-space pathways contributing to the third-order optical response of a V-type system. The pathways for the rephasing spectrum $S_I(\omega_\tau,T,\omega_t)$ and Raman spectrum $S_I(\tau,\omega_T,\omega_t)$ are listed in the top two rows; the pathways for the nonrephasing spectrum $S_{II}(\omega_\tau,T,\omega_t)$ are listed in bottom two rows. The state numbers, 0, 1, and 2, correspond to $4^2S_{1/2}$, $4^2P_{1/2}$, and $4^2P_{3/2}$ of potassium atoms.

relative values of 1:2:2:4. Similarly, the peak strength ratio in the $S_{II}(\omega_\tau,T,\omega_t)$ measurement NA:NC:ND:NB is equal to 2:1:1:5, which agrees well with the experimental result.

The interaction between light and a closed two-level system can be described by the optical Bloch equations [36]:

$$\dot{\rho}_{00} = -\dot{\rho}_{11}, \tag{1}$$

$$\dot{\rho}_{11} = -\gamma^{sp}\rho_{11} + \frac{i}{\hbar}\mu_{01}E(\rho_{01}-\rho_{10}), \tag{2}$$

$$\dot{\rho}_{01} = -\gamma^{ph}\rho_{01} + i\omega_{01}\rho_{01} + \frac{i}{\hbar}\mu_{01}E(\rho_{11}-\rho_{00}), \tag{3}$$

where ρ_{00} and ρ_{11} are density matrix elements for the ground- and excited-state population, respectively, and ρ_{01} is the

off-diagonal term of the density matrix. γ^{sp} and γ^{ph} are the population relaxation and dephasing rates, respectively, μ_{01} is the transition dipole moment, ω_{01} is the resonant transition frequency, and E is the electric field amplitude. We extended the equations to a multilevel system and numerically solved them [37,38]. In the calculation, γ^{ph} is the total linewidth due to resonance and collision broadening. The induced polarization of the system is $P = N\mathrm{tr}(\mu\rho)$. Then the electric field of the emitted signal is determined from the third-order polarization [37]:

$$E(\tau,T,\omega_t) = \frac{2\pi L}{n(\omega_t)c} i\omega_t P^{(3)}(\tau,T,\omega_t) \tag{4}$$

where L is the sample thickness, $n(\omega_t)$ is the index of refraction of the sample, and c is the speed of light in vacuum. $S_I(\omega_\tau,T,\omega_t)$ and $S_{II}(\omega_\tau,T,\omega_t)$ 2DFT spectra are defined as the Fourier transform with respect to delay τ:

$$S_{I,II}(\omega_\tau,T,\omega_t) = \int_{-\infty}^{\infty} E(\tau,T,\omega_t)\, e^{i\omega_\tau\tau} d\tau. \tag{5}$$

The numerical simulations of the $S_I(\omega_\tau,T,\omega_t)$ and $S_{II}(\omega_\tau,T,\omega_t)$ spectra shown in Fig. 4 are in very good agreement with the experiment; correct peak strengths and symmetric starlike line shapes are reproduced in the amplitude spectra, indicating the dominance of homogeneous broadening [32]. As expected, the line shapes are mainly absorptive, which is in contrast to semiconductors, where many-body interactions result in dispersive line shapes [20,24,38].

While the line shapes in the $S_I(\omega_\tau,T,\omega_t)$ and $S_{II}(\omega_\tau,T,\omega_t)$ spectra are mainly absorptive, there are weak dispersive contributions. Purely absorptive contributions can be isolated by adding the $S_I(\omega_\tau,T,\omega_t)$ and $S_{II}(\omega_\tau,T,\omega_t)$ signals together [18,39]. The experimental and theoretical purely absorptive spectra are shown in Fig. 5. Compared with the $S_I(\omega_\tau,T,\omega_t)$ and $S_{II}(\omega_\tau,T,\omega_t)$ spectra, the disappearance of dispersive wings in the purely absorptive spectra results in a higher resolution of spectral features.

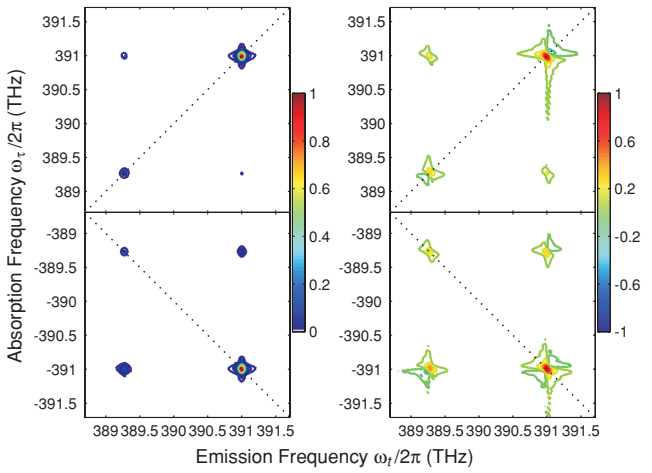

FIG. 4. (Color) Calculated amplitude (left) and real-part (right) 2DFT spectra of potassium vapor for $S_I(\omega_\tau,T,\omega_t)$ (bottom) and $S_{II}(\omega_\tau,T,\omega_t)$ (top) measurements. The spectra are normalized to the most intense peaks.

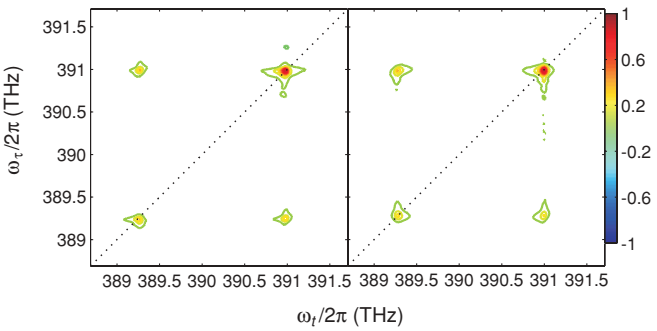

FIG. 5. (Color) Experimental (left) and theoretical (right) purely absorptive spectra obtained by the addition of the $S_I(\omega_\tau,T,\omega_t)$ and $S_{II}(\omega_\tau,T,\omega_t)$ spectra.

Cross peaks in $S_I(\omega_\tau,T,\omega_t)$ have contributions from ground-state bleaching and excited-state emission pathways. These two pathways differ during the delay time T. After the second excitation pulse, the ground-state bleaching pathway leaves the system in the ground state, while the excited-state emission or Raman-like pathway (labeled TC or TD in Fig. 3) leaves the system in a coherent superposition of $4^2P_{1/2}$ and $4^2P_{3/2}$. $S_I(\tau,\omega_T,\omega_t)$ spectra can be used to isolate Raman coherence terms, projecting the 2DFT signal along ω_T and ω_t instead of ω_τ and ω_t [21]. Technically, the measurement is achieved by scanning the third pulse C while keeping the time delay τ between first two pulses constant. The spectrum is then obtained by fast Fourier transform of time domain signal with respect to T. Figure 6 shows an experimental spectrum of $S_I(\tau,\omega_T,\omega_t)$, with $\tau = 0$ in the measurement. In the spectrum, two strong peaks are observed along the zero mixing energy, and two side peaks show up at the energy position of TC $(E_{D2}, E_{D2} - E_{D1})$ and TD $(E_{D1}, E_{D1} - E_{D2})$, where E_{D1} and E_{D2} are the photon energies corresponding

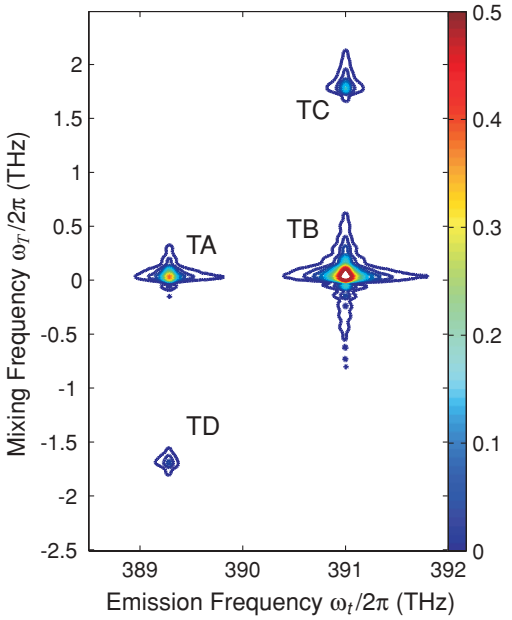

FIG. 6. (Color) Experimental amplitude $S_I(\tau,\omega_T,\omega_t)$ spectrum.

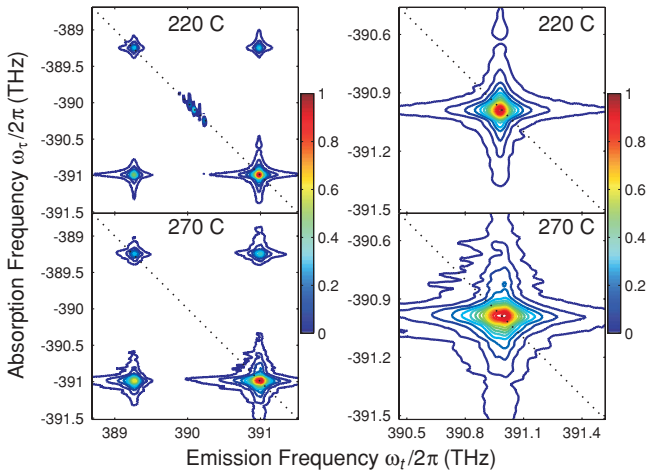

FIG. 7. (Color) Distortion of the peak shapes due to propagation effects. Left panels are the $S_I(\omega_\tau,T,\omega_t)$ spectra of the potassium vapor at 220 °C (top) and 270 °C (bottom). Right panels are the zoomed pictures of the diagonal peaks corresponding to the D_2 transition at 220 °C (top) and 270 °C (bottom).

to the transitions D_1 and D_2 separately. The amplitude of the spectrum is normalized according to the strength of the strongest peak; however, the spectrum is displayed with a color scale of 0 to 0.5 to emphasize two side peaks. It is clear that the two quantum pathways for Raman coherences (TC and TD) can be isolated as two side peaks in the $S_I(\tau,\omega_T,\omega_t)$ spectrum. Weak asymmetry between TC and TD features is observed, where the stronger peak has the same emission energy as the stronger zero mixing energy feature. This asymmetry is also observed in semiconductors [21].

The dephasing rate of the Raman coherence is related to the dephasing rates of the optical transitions by [40]

$$\gamma_{D2-D1} = \gamma_{D2} + \gamma_{D1} - 2R_{ph}(\gamma_{D1}\gamma_{D2})^{1/2}, \tag{6}$$

where γ_{D2-D1}, γ_{D2}, and γ_{D1} are the dephasing rates for the Raman coherences, the D_2 and D_1 transitions, respectively. The coefficient R_{ph} describes the degree of correlation between fluctuations of the two transitions. The dephasing rates of D_2 and D_1 extracted from the $S_I(\omega_\tau,T,\omega_t)$ measurement are 0.128 and 0.118 THz. The dephasing rates for the Raman coherences at the energy position of TC and TD are 0.127 and 0.140 THz, respectively, so the correlation coefficients R_{ph} are 0.45 and 0.43, respectively. The positive correlation coefficients means that the energies of the D_2 and D_1 lines simultaneously shift in the same direction relative to each other during the collisional scattering, as expected. These results show that 2DFT spectroscopy can make a quantitative determination of the correlation between fluctuations of two excited levels in atomic systems.

As in other types of spectroscopy, the line shapes in 2DFT spectroscopy can be affected by the propagation of the excitation laser pulses and signals in the resonant medium. Propagation effects in TFWM experiments of alkali-metal vapors have been discussed [5], as have distortions of 2DFT spectra due to propagation effects [41–44]. When the number density of atomic potassium is increased by raising the temperature, the absorption also strengthens. Distortion of 2DFT spectra peaks due to propagation can then be observed. $S_I(\omega_\tau,T,\omega_t)$ spectra of potassium vapor at 220 and 270 °C are shown in Fig. 7, where the absorbance αL is ~0.2 and ~1.3 for the D_2 transitions at those temperatures, respectively. At the lower temperature, the diagonal D_2 feature is a symmetric star shape, while at high temperature it is elongated along the emission photon axis. This change has been predicted [41–43], although the expected change in peak strength ratio is not observed [41].

IV. CONCLUSION

$S_I(\omega_\tau,T,\omega_t)$ and $S_{II}(\omega_\tau,T,\omega_t)$ 2DFT spectra for potassium vapor have been obtained using a multidimensional nonlinear spectrometer. Numerical simulation based on the optical Bloch equations reproduce the experimental spectra, giving excellent agreement. Purely absorptive spectra are obtained by summing $S_I(\omega_\tau,T,\omega_t)$ and $S_{II}(\omega_\tau,T,\omega_t)$. We also experimentally isolated Raman coherences by projecting the 2DFT signal along ω_T and ω_t instead of ω_τ and ω_t and calculated the correlation between fluctuations of the D_1 and D_2 transitions. Finally, the expected distortion of 2DFT spectra due to propagation effect is observed at higher vapor temperatures.

2DFT spectroscopy has been proved to be a powerful tool to show interactions and couplings in complex systems. However, those spectra are often very complicated and the line shapes can be severely distorted for various reasons [43] and quantitative analysis is generally difficult for those spectra. Simple atomic systems, such as the potassium vapor system studied in this paper, can be excellent test beds to study the distortions of the line shapes in 2DFT spectroscopy. On the other hand, the 2DFT technique can be a new spectroscopic method to study the interactions in simple atomic and molecular systems. As we have demonstrated, the technique can directly show the couplings and correlations between different energy levels or transitions and provide quantitative information for those couplings and correlations. When energy level structures are more complex, the 2DFT technique will be more promising than traditional spectroscopic techniques, since all spectroscopic information can be extracted from one single spectrum due to the spectral characteristic of ultrafast laser pulses. In addition, our preliminary experimental results show that another type of 2DFT spectrum called the S_{III} spectrum, which has been recently demonstrated in semiconductor quantum wells [27], can also detect the couplings between different atoms. In summary, we conclude that 2DFT spectroscopy of simple systems can be useful to validate various techniques and theories for 2DFT spectroscopy, and the 2DFT technique can be an equally powerful tool to study the interactions and couplings in simple quantum systems as well as complex systems.

ACKNOWLEDGMENTS

The authors thank T. Asnicar and H. Green for technical assistance. The financial support is provided by NIST and the National Science Foundation's Physics Frontier Center Program.

[1] I. Bloch, J. Dalibard, and W. Zwerger, Rev. Mod. Phys. **80**, 885 (2008).
[2] M. Fleischhauer, A. Imamoglu, and J. Marangos, Rev. Mod. Phys. **77**, 633 (2005).
[3] A. Flusberg, T. Mossberg, R. Kachru, and S. R. Hartmann, Phys. Rev. Lett. **41**, 305 (1978).
[4] O. Kinrot and Y. Prior, Phys. Rev. A **50**, 1999(R) (1994).
[5] O. Kinrot and Y. Prior, Phys. Rev. A **51**, 4996 (1995).
[6] J. Golub and T. Mossberg, J. Opt. Soc. Am. B **3**, 554 (1986).
[7] F. Shen, J. Gao, A. A. Senin, C. J. Zhu, J. R. Allen, Z. H. Lu, Y. Xiao, and J. G. Eden, Phys. Rev. Lett. **99**, 143201 (2007).
[8] V. O. Lorenz and S. T. Cundiff, Phys. Rev. Lett. **95**, 163601 (2005).
[9] V. O. Lorenz, S. Mukamel, W. Zhuang, and S. T. Cundiff, Phys. Rev. Lett. **100**, 013603 (2008).
[10] S. Mukamel, Annu. Rev. Phys. Chem. **51**, 691 (2000).
[11] R. R. Ernst, G. Bodenhausen, and A. Wokaun, *Principles of Nuclear Magnetic Resonance in One and Two Dimensions* (Clarendon, Oxford, 1987).
[12] Y. Tanimura and S. Mukamel, J. Chem. Phys. **99**, 9496 (1993).
[13] M. Cho, Chem. Rev. **108**, 1331 (2008).
[14] M. D. Fayer, D. E. Moilanen, D. Wong, D. E. Rosenfeld, E. E. Fenn, and S. Park, Acc. Chem. Res. **42**, 1210 (2009).
[15] T. Elsaesser, Acc. Chem. Res. **42**, 1220 (2009).
[16] P. Tian, D. Keusters, Y. Suzaki, and W. Warren, Science **300**, 1553 (2003).
[17] J. C. Vaughan, T. Hornung, K. W. Stone, and K. A. Nelson, J. Phys. Chem. A **111**, 4873 (2007).
[18] P. F. Tekavec, G. A. Lott, and A. H. Marcus, J. Chem. Phys. **127**, 214307 (2007).
[19] N. S. Ginsberg, Y.-C. Cheng, and G. R. Fleming, Acc. Chem. Res. **42**, 1352 (2009).
[20] S. T. Cundiff, T. Zhang, A. D. Bristow, D. Karaiskaj, and X. Dai, Acc. Chem. Res. **42**, 1423 (2009).
[21] L. Yang, T. Zhang, A. D. Bristow, S. T. Cundiff, and S. Mukamel, J. Chem. Phys. **129**, 234711 (2008).
[22] A. D. Bristow, D. Karaiskaj, X. Dai, T. Zhang, C. Carlsson, K. R. Hagen, R. Jimenez, and S. T. Cundiff, Rev. Sci. Instrum. **80**, 073108 (2009).
[23] A. D. Bristow, D. Karaiskaj, X. Dai, and S. T. Cundiff, Opt. Express **16**, 18017 (2008).
[24] A. D. Bristow, D. Karaiskaj, X. Dai, R. P. Mirin, and S. T. Cundiff, Phys. Rev. B **79**, 161305(R) (2009).
[25] K. W. Stone, K. Gundogdu, D. B. Turner, X. Li, S. T. Cundiff, and K. A. Nelson, Science **324**, 1169 (2009).
[26] L. Yang and S. Mukamel, Phys. Rev. Lett. **100**, 057402 (2008).
[27] D. Karaiskaj, A. D. Bristow, L. Yang, X. Dai, R. P. Mirin, S. Mukamel, and S. T. Cundiff, Phys. Rev. Lett. **104**, 117401 (2010).
[28] V. O. Lorenz, X. Dai, H. Green, T. R. Asnicar, and S. T. Cundiff, Rev. Sci. Instrum. **79**, 123104 (2008).
[29] E. Fiock and W. Rodebush, J. Am. Chem. Soc. **48**, 2522 (1926).
[30] E. Lewis, M. Rebbeck, and J. Vaughan, J. Phys. B **4**, 741 (1971).
[31] N. Lwin and D. Mccartan, J. Phys. B **11**, 3841 (1978).
[32] S. Faeder and D. Jonas, J. Phys. Chem. A **103**, 10489 (1999).
[33] I. Kuznetsova, T. Meier, S. T. Cundiff, and P. Thomas, Phys. Rev. B **76**, 153301 (2007).
[34] M. E. Siemens, G. Moody, H. Li, A. D. Bristow, and S. T. Cundiff, Opt. Express **18**, 17699 (2010).
[35] L. Lepetit, G. Cheriaux, and M. Joffre, J. Opt. Soc. Am. B **12**, 2467 (1995).
[36] L. Allen and J. Eberly, *Optical Resonance and Two-Level Atoms* (Dover, New York, 1987).
[37] J. M. Shacklette and S. T. Cundiff, J. Opt. Soc. Am. B **20**, 764 (2003).
[38] X. Li, T. Zhang, C. N. Borca, and S. T. Cundiff, Phys. Rev. Lett. **96**, 057406 (2006).
[39] M. Khalil, N. Demirdoven, and A. Tokmakoff, Phys. Rev. Lett. **90**, 047401 (2003).
[40] A. G. V. Spivey, C. N. Borca, and S. T. Cundiff, Solid State Commun. **145**, 303 (2008).
[41] D. Keusters and W. Warren, J. Chem. Phys. **119**, 4478 (2003).
[42] D. Keusters and W. Warren, Chem. Phys. Lett. **383**, 21 (2004).
[43] M. K. Yetzbacher, N. Belabas, K. A. Kitney, and D. M. Jonas, J. Chem. Phys. **126**, 044511 (2007).
[44] K. Kwak, D. E. Rosenfeld, and M. D. Fayer, J. Chem. Phys. **128**, 204505 (2008).